ARTICLES

Separation of the $^2H(e,e'p)$ structure functions up to 0.9 GeV/c momentum transfer

J. E. Ducret, M. Bernheim, J. F. Danel, L. Lakehal-Ayat, J. M. Le Goff,
A. Magnon, C. Marchand, J. Morgenstern, and P. Vernin
DAPNIA/Service de Physique Nucléaire, Centre d'Etudes de Saclay, 91191 Gif sur Yvette, France

M. K. Brussel
Department of Physics, University of Illinois, Urbana, Illinois 61801

H. Arenhövel, G. Beck, and T. Wilbois
Institut für Kernphysik der Universität Mainz, 55099 Mainz, Germany

G. P. Capitani and E. De Sanctis
Laboratori Nazionali di Frascati, Istituto Nazionale di Fisica Nucleare, I-00044 Frascati, Italy

S. Frullani, F. Garibaldi, F. Ghio, and M. Jodice
Laboratori di Fisica, Istituto Superiore di Sanita
and Istituto Nazionale di Fisica Nucleare, Sezione Sanita, I-00161 Roma, Italy

(Received 6 October 1993)

Longitudinal, transverse, and longitudinal-transverse structure functions for the $^2H(e,e'p)$ reaction have been determined. Measurements of the cross sections were made in-plane in nearly quasielastic kinematics spanning momentum transfers between 200 and 670 MeV/c and recoil momenta between 0 and 150 MeV/c. In addition, cross sections at momentum transfers above 800 MeV/c were measured at backward scattering angles in aligned kinematics where the response is predominantly transverse. We compared our data with both relativistic and nonrelativistic models. Our results are not consistently in agreement with any of the calculations based on these models. The disagreement between our data and these calculations ranges from 0% to 30%; on average it is about 10%. Notable discrepancies arise in describing relativistic effects for the longitudinal-transverse structure function, at a momentum transfer of 400 MeV/c as well as for the transverse structure function at momentum transfer above 800 MeV/c.

PACS number(s): 21.45.+v, 25.10.+s, 25.30.Fj

I. INTRODUCTION

Electron scattering has long proved to be a preferred technique to probe nuclear structure. The weakness of electromagnetic forces permits rapidly converging pertubative calculations of the cross sections. The success of the technique is exemplified by the great accuracy with which nuclear charge and magnetization densities have been determined [1].

In *inclusive* scattering experiments, only the scattered electrons are detected. Above the peaks corresponding to elastic scattering and excitation of the giant resonances, the energy loss spectrum for intermediate beam energies exhibits a broad feature called the quasielastic (QE) peak. It is understood to be due to the incoherent scattering of the electrons from individual moving nucleons of the target nucleus [2]. If these nucleons emerge from the nucleus, they can be detected *in coincidence* with the scattered electrons. In the work reported here, we have studied those coincidence events in which a proton emerges. An advantage of such $(e,e'p)$ *exclusive* measurements is their selectivity; in contrast to the inclusive reaction where only an average over processes which can include many nucleons is sensed, the coincidence measurement allows the initial state of the detected proton inside the target nucleus to be inferred, as long as it is further assumed that any struck nucleon exits from the system without further interaction [the so-called plane wave impulse approximation (PWIA)]. The dynamics of the electron-nucleon interaction and the properties of the target nucleus can then be checked within the context of quasielastic reaction models.

The *inclusive* (e,e') cross section is the sum (if Coulomb distortion is ignored) of two response functions, longitudinal (L) and transverse (T), which correspond to the different polarization states of the exchanged virtual photon [3]. Each harbors specific information about the reaction, the longitudinal response being related to the charge and the transverse to the magnetic properties of the nucleus. In recent years, these response functions have been determined experimentally for a wide variety of nuclei, from ^2H to ^{238}U [4–23]. Except for the lightest nuclei, ^2H, ^3H, and ^3He [14–18] and for the recent data on ^{40}Ca from Yates *et al.* [23] which are in disagreement with the data from Saclay [11–13], a noticeable reduction of the longitudinal response function relative to the transverse has been observed [24] in the vicinity of the quasielastic peak. The reduction varies from 35% in ^4He

[20] to 60% in ^{208}Pb [19]. In PWIA calculations, such reductions are absent: The observed transverse response at the QE peak is fairly well reproduced, but the longitudinal response is generally overestimated. These effects are not well understood.

The PWIA calculations have been refined by incorporating both short and long range nucleon-nucleon correlations [25,26] and relativistic nuclear dynamics [30–34]. These effects tend to succeed in reducing the longitudinal response function relative to the transverse [24]. Modifications of the nucleon properties in the nucleus, which change the basic electron-bound nucleon coupling [30–34], have also been considered as a way to explain the reduced longitudinal response.

When trying to unravel the various mechanisms involved in the $(e,e'p)$ reaction, much can be learned from a structure function decomposition of the cross sections, paralleling experience with the inclusive reaction where Rosenbluth separations revealed unsuspected behavior of the longitudinal and the transverse responses. For example, it would seem straightforward, in the context of the PWIA, to verify whether bound nucleons exhibit magnetic and elastic form factors different from those of free nucleons. One would simply fix the $(e,e'p)$ kinematics to maintain nuclear effects constant and measure the momentum transfer dependence of the structure functions, as in the standard procedure used in measurements of the free nucleon electric and magnetic form factors.

In kinematics for which the proton is ejected from the nucleus in the direction of the exchanged photon (aligned kinematics), the exclusive $(e,e'p)$ cross section is the sum of longitudinal and transverse structure functions, as in the inclusive case. The separation of these structure functions has been achieved for ^{2}H, ^{6}Li, and ^{12}C at NIKHEF [35–38], for ^{12}C at Bates [39] and for ^{40}Ca and ^{4}He [40–43] at Saclay. For ^{40}Ca, the longitudinal and the transverse structure functions revealed a Q^2 dependence compatible with that of the free proton. However, even after model-dependent corrections for rescattering of the ejected proton by the residual nucleus which affect the two structure functions differently, the longitudinal response was still reduced relative to the transverse by about 30%. This result is consistent with the inclusive results on this nucleus [13]. To better understand and to complement these results, we decided to replicate the experiment on ^{4}He which, with its relatively large density and binding energy, resembles heavier nuclei. The structure functions for the ^{4}He$(e,e'p)^{3}$H reaction were separated in aligned and nearly QE kinematics [42,43]. A 35% suppression of the longitudinal structure function (normalized to that of the free proton) relative to the (normalized) transverse was observed, similar to the case of ^{40}Ca. This suppression was reduced to 20% after model-dependent corrections for final state interactions were applied.

In view of the unexplained inequality of the normalized $(e,e'p)$ structure functions on ^{40}Ca and ^{4}He, we may question our fundamental understanding of the $(e,e'p)$ reaction: (1) How well known are the ground state nuclear wave functions? (2) Can we accurately describe the effects of rescattering, charge exchange, meson exchange, and isobaric excitations? (3) Do we need to revise the impulse approximation description of the reaction? (4) Ought we to use free form factors for the bound protons? (5) How should we account for relativistic effects? A straightforward way to investigate these questions at the most fundamental nuclear level is to make similar measurements on ^{2}H and ^{3}He.

^{2}H and ^{3}He have average densities and binding energies several times smaller than ^{4}He. Their wave functions can be precisely computed even in the final continuum state, in contrast to ^{4}He. Experimentally, no significant differences between the longitudinal and transverse response functions have been observed for the inclusive reaction on ^{2}H and ^{3}He, suggesting that these reactions are more prototypically quasielastic.

In the simplest case, deuterium, calculational uncertainties ought to be minimal: (1) The nonrelativistic wave function can be computed precisely from realistic nucleon-nucleon potentials; (2) the proton in deuterium is weakly bound (E_b=2.2 MeV), implying a minimal ambiguity in the off-shell nature of the electron-nucleon coupling; and (3) reaction mechanism effects supplementary to the PWIA can be accounted for with relatively good accuracy.

At Saclay, we have completed $(e,e'p)$ experiments on both ^{2}H and ^{3}He [44–46]. This paper concerns our results on deuterium. Its outline is as follows: In Sec. II, the formalism necessary to describe the reaction is given. In Sec. III, the experimental apparatus, the systematic errors, and the kinematics of the measurements are discussed. In Sec. IV, our results are presented and compared to theoretical models and to other ^{2}H$(e,e'p)$ experiments. Conclusions are stated in Sec. V.

II. FORMALISM

The simplest description of the $(e,e'p)$ reaction employs the plane wave impulse approximation (PWIA) [47]. This approximation assumes that the electron couples to only one proton of the target nucleus and that this proton is ejected from the nucleus without further interacting.

In the PWIA, the $(e,e'p)$ cross section can be factored into two terms: one representing the elementary electron-bound proton cross section $\sigma_{(e\text{-}p)}$ and the other the probability density $S(p,E_m)$ for finding a proton of momentum $p=|\mathbf{p}|$ and missing energy (or separation energy) E_m within the nucleus [48]:

$$\frac{d^4\sigma}{de'd\Omega_{e'}dp'd\Omega_{p'}}=\sigma_{(e\text{-}p)}S(p,E_m). \tag{1}$$

The kinematics of the $(e,e'p)$ reaction is defined as follows: $e=(e,\mathbf{e})$ and $e'=(e',\mathbf{e}')$ denote the four-momenta of the incident and scattered electrons in the limit $m_e \ll e,e'$. $P'=(E_{p'},\mathbf{p}')$ is the four-momentum of the ejected proton and $P_r=(E_r,\mathbf{p}_r)$ is the four-momentum of the recoiling residual nucleus. In the PWIA, the initial momentum $\mathbf{p}$ of the ejected proton in the target nucleus is equal and opposite to $\mathbf{p}_r$: $\mathbf{p}=-\mathbf{p}_r$. $\mathbf{p}_r$ is therefore a key

parameter of $(e,e'p)$ reactions, for it is measurable, and it reflects the initial momentum of the struck nucleon. $Q = (\omega, \mathbf{q})$ is the momentum transfer four-vector, and $Q^2 \equiv \mathbf{q}^2 - \omega^2$ gives its magnitude.

E_m, the missing energy, is defined as

$$E_m = M_p + M_r^* - M_A, \tag{2}$$

where M_p, M_r^*, and M_A are the proton, residual nucleus (possibly excited, indicated by the asterisk), and target nucleus masses, respectively. For the ^{2}H$(e,e'p)n$ reaction, M_r is the neutron mass and E_m=2.2 MeV.

$S(p,E_m)$ is directly related to the nuclear wave function. In the PWIA, it contains all the nuclear structure information that can be extracted from $(e,e'p)$ cross sections. As already implied, the knockout of an individual nucleon which exits the nucleus unimpeded is only an approximation; in reality, more complicated reaction mechanisms are involved. To take these into account, the factorization of Eq. (1) is abandoned and the $(e,e'p)$ reaction is considered in the more general framework of the Born approximation (BA) where the only assumption made is that energy and momentum are transferred from the electron to the nucleus by the exchange of a single virtual photon. In particular, nothing is assumed about the structure of the electromagnetic nuclear current, whereas in the PWIA this current is a sum of plane waves.

In the BA, the $(e,e'p)$ cross section can be decomposed in terms related to the polarization states of the exchanged photon. The expression for the cross section can be written [49]

$$\frac{d^4\sigma}{de'd\Omega_{e'}dp'd\Omega_{p'}} = \Gamma(\sigma_T + \varepsilon\sigma_L + \sqrt{\varepsilon(\varepsilon+1)}\sigma_{TL}\cos\phi + \varepsilon\sigma_{TT}\cos 2\phi). \tag{3}$$

The subscripts L and T refer to the longitudinal (along $\mathbf{q}$) and the transverse (orthogonal to $\mathbf{q}$) polarization states of the photon. In Eq. (3), the σ_α, $\alpha = L$, T, TL, TT are the $(e,e'p)$ *structure functions*; they depend only on $q = |\mathbf{q}|$, ω, $|\mathbf{p}'|$, and $\theta_{p'q}$, the angle between $\mathbf{p}'$ and $\mathbf{q}$. σ_{TL} and σ_{TT} arise from the interference of the longitudinal and the transverse components of the nuclear current operator. ϕ is the angle between the electron scattering plane and the plane defined by $\mathbf{p}'$ and $\mathbf{p}_r$. The longitudinal polarization of the virtual photon is given by

$$\varepsilon = \left[1 + 2\frac{\mathbf{q}^2}{Q^2}\tan^2\left(\frac{\theta_{e'}}{2}\right)\right]^{-1}. \tag{4}$$

ε lies between 0 and 1. The flux of virtual photons in the laboratory frame is given by

$$\Gamma = \frac{\alpha}{2\pi^2}\frac{e'}{e}\frac{|\mathbf{q}|}{Q^2}\frac{1}{1-\varepsilon}. \tag{5}$$

Formula (3) is valid only when $Z\alpha \ll 1$, Z being the charge number of the target nucleus and α the fine structure constant. It does not take into account second order terms [in $(Z\alpha)^2$] which represent the distortion of the electron wave function in the Coulomb field of the target nucleus [50,51]. For light nuclei ($Z \leq 2$), these terms amount to about 2% of the BA cross section. However, the present cross sections were corrected for Coulomb distortion during the data analysis.

In aligned kinematics, where $\mathbf{q}$ and $\mathbf{p}'$ are parallel ($\theta_{p'q} = 0$), the interference structure functions σ_{TL} and σ_{TT} vanish. The $(e,e'p)$ cross section then reduces to two structure function terms which can be separated using the Rosenbluth method [52] by measuring two cross sections at constant q, ω, and $|\mathbf{p}'|$: one at a high incident energy and a forward electron scattering angle where $\varepsilon \simeq 0.5$–0.8, the other at a lower energy and a backward angle where $\varepsilon \simeq 0.1$–0.2. In the general case ($\theta_{p'q} \neq 0$), the four structure functions can be determined with independent measurements of the cross sections at different values of ϕ and ε, again maintaining q, ω, p', and $\theta_{p'q}$ constant: This necessitates out-of-plane ($\phi \neq 0, \pi$) proton detection. However, the σ_{TL} interference structure function can be extracted by in-plane measurements alone ($\phi = 0, \pi$). σ_{TT} can be determined only by out-of-plane measurements [53], but since for small values of $\theta_{p'q}$ its contribution is small, its effect on the determination of the other structure functions can be approximated using a simple PWIA model. The three structure functions σ_T, σ_L, and σ_{TL} can then be separated with two forward angle measurements, at $\phi = 0$ and at $\phi = \pi$, and a single backward angle measurement.

If we apply the BA to the elementary electron-bound proton cross section, we can expand $\sigma_{(e\text{-}p)}$ in terms related to the polarization states of the exchanged photon, just as for the $(e,e'p)$ cross section, giving rise to four elementary structure functions $\sigma^\alpha_{(e\text{-}p)}$ ($\alpha = L$, T, TL, TT). Then, having determined the nuclear structure functions σ_α and using a model for $\sigma_{(e\text{-}p)}$, we may define four *experimental spectral functions* by the ratios

$$S^{\text{expt}}_\alpha = \frac{\sigma_\alpha}{\sigma^\alpha_{(e\text{-}p)}}, \quad \alpha = L, T, TL, TT. \tag{6}$$

In the PWIA, the σ_α factorize and all the spectral functions are the same:

$$S^{\text{expt}}_L = S^{\text{expt}}_T = \cdots = S(p,E_m). \tag{7}$$

The PWIA does not provide the most accurate description of $(e,e'p)$ reactions. One has to take into account the fact that the proton is not free in the initial state and that multibody contributions in the electromagnetic nuclear current operator such as meson exchange currents (MEC's) may not be negligible. Moreover, final state interactions such as charge exchange and nucleon rescattering after the absorption of the virtual photon may be important [54]. The structure functions embed different components of the electromagnetic nuclear currents and have different sensitivities to various $(e,e'p)$ reaction mechanisms. They then depend on E_m, p_r, q, and ω in a nonfactorizable way. The result is that they may induce a q and ω dependence onto the S^{expt}_α and break the equality between the S^{expt}_α that occurs in the PWIA [Eq. (7)].

The goal of the present ^{2}H$(e,e'p)$ experiment has been to study the possible dependence of the $S_\alpha^{\rm expt}$ on p_r, q, and ω near the QE peak in a kinematical range as wide as possible. To compute these experimental spectral functions from the $(e,e'p)$ structure functions, we have chosen the cc1 prescription of de Forest for $\sigma_{(e\text{-}p)}$ because it is gauge invariant and uses relativistic kinematics [55]. In this model of the electron-bound proton cross section, the free proton form factors are used.

III. SACLAY ^{2}H$(e,e'p)$ EXPERIMENT

A. Experimental setup

This experiment was performed at the linear accelerator of Saclay (A.L.S.), in the HE1 end station. The A.L.S. provided electron beams of energy between 100 and 720 MeV, with a duty cycle of 0.5% above 400 MeV and 2% below 400 MeV.

The HE1 end station is equipped with two high resolution magnetic dipole spectrometers, the 600 and the 900, the names referring to the maximum momentum in MeV/c which they can accept. The properties of these spectrometers and other information about HE1 are described in other references [56–59] and will not be detailed here.

We used a liquid deuterium target, similar to one described in [60]. This target is cooled, through a heat exchanger by a primary circuit of liquid hydrogen at 20 K. The deuterium target proper consists of a cylinder of 35 mm high and 15 mm in diameter and forms part of the secondary cryogenic circuit.

This target features thin walls (0.02 mm thick stainless steel) and high stability. The wall thickness in radiation lengths, 1.14×10^{-3}, was equivalent to that of the half transversal (radius) of the liquid deuterium target. Only 10% of the total proton energy loss occurred in traversing the wall. Luminosities between 5×10^{35} and 5×10^{36} cm^{-2} s^{-1} could be tolerated without incurring excessive radiative corrections (see below) to the experimental counting rates. The variations of target density from beam heating were less than 0.3%/μA, due to the relatively good thermal conductivity of the liquid deuterium and the quality of the target heat exchanger. We could then take data with average beam currents as high as 12 μA.

Crucial to this experiment was the accuracy with which we could determine the recoil momentum $\mathbf{p}_r$. Because of the steep slope of the spectral function, the ^{2}H$(e,e'p)$ cross section depends strongly on $\mathbf{p}_r$ as

$$\frac{1}{\sigma_{(e,e'p)}} \frac{\partial \sigma_{(e,e'p)}}{\partial p_r} \simeq 2 - 4\%/(\text{MeV}/c), \tag{8}$$

the precise value depending on the magnitude of the recoil momentum. In order to accurately reconstruct $\mathbf{p}_r$ from the measured variables, we were led to add a small amount of hydrogen, around 0.5% (in mass), to the liquid deuterium; we could then monitor *in situ* the kinematical variables through the ^{1}H$(e,e'p)$ reaction. The hydrogen elastic scattering events are characterized by $E_m = 0$ and $\mathbf{p}_r = \mathbf{0}$ and were used to calibrate the reconstruction of $\mathbf{p}_r$. They were within the experimental acceptance when the detection system was tuned on low recoil momentum deuterium kinematics. Since E_m=2.2 MeV for ^{2}H$(e,e'p)$, we could distinguish the two reactions experimentally in a missing energy spectrum (see Fig. 1) by parametrizing the left side of the two-body breakup (in the following designated as 2BBU) peak with a Gaussian curve and subtracting it from the experimental histogram; the difference was attributed to ^{1}H$(e,e'p)$ events. Once these events were selected, the associated energy losses of the particles in the deuterium and the target and spectrometer windows were calculated to obtain the vertex energies. The recoil momentum $\delta\mathbf{p}_r$ of the ^{1}H$(e,e'p)$ events, reconstructed using the vertex momenta in the equation

$$\delta\mathbf{p}_r = \mathbf{e} - \mathbf{e}' - \mathbf{p}' \,, \tag{9}$$

then gives a measure of the accuracy in $\mathbf{p}_r$ achievable in the kinematics reconstruction.

In our experiment, outgoing proton momenta ranged from 300 to 800 MeV/c. At p'=300 MeV/c, the protons lost approximately 10 MeV/c in traversing half of the deuterium target (7.5 mm). In order to accurately correct for the energy losses in the target material, we controlled the beam position at the target with a beam monitoring system consisting of two beam position monitors, one 10 cm and the other 8 m downstream from the target center. A feedback loop from the monitor nearest the target ensured that the beam always passed through its center. Information on the centroid of the beam from the more downstream (beam profile) monitor [61] allowed us to determine the beam direction and position at the target. Knowledge of the incident beam direction was also important in enabling us to reconstruct $\mathbf{p}_r$. An error $\delta\theta$ in the direction of the incident beam induces an error $\delta p_r = e\delta\theta$ on the recoil momentum [Eq. (9)]. A 1 cm shift of the 700 MeV beam observed on the beam profile monitor corresponded to a transverse shift of the beam at the target center of 0.13 mm (thus negligible in terms of energy loss) and to an error in the recoil momentum of $\sim$ 0.8 MeV/c. During the experiment, we readjusted the beam steering whenever it deviated by more than 0.5 cm on the beam monitor.

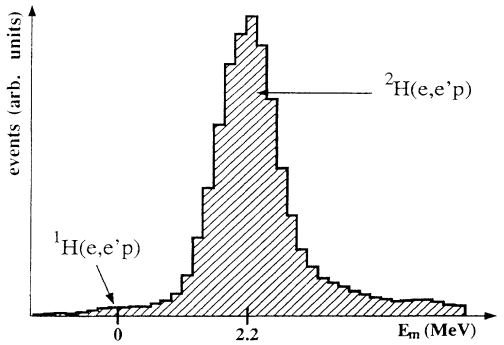

FIG. 1. Typical missing energy spectrum of our ^{2}H$(e,e'p)$ experiment.

B. Data analysis

Accidental events were subtracted from beneath the peak of $(e,e'p)$ events by histogramming the time difference of all proton-electron coincidence events. This histogram, after corrections for electron-proton time of flight differences, consisted of the peak of time-correlated events, 1.5 ns in width [full width at half maximum (FWHM)], and a constant background of uncorrelated events [43]. The accidental contribution to the coincidence peak was determined from this constant background on both sides of the coincidence peak, and could be easily subtracted to obtain the true event rate.

The counting rates were corrected for electronics dead time and inefficiencies. The associated losses were less than 25% of the counting rate and were determined with fast scalers at different points in the electronics to an absolute accuracy of 1%. We corrected for the beam-induced variations of the target density by using the proton trigger rate in the 900 spectrometer as a monitor. This was feasible by the very low level of background in this trigger; every trigger signal in the 900 originated from the target. Thus, the 900 trigger rate, normalized to the average beam current, was proportional to the real density. The target density variations with the beam current were less than $0.3\%/\mu$A. Once corrected, they contribute negligible systematic error on the determination of the $(e,e'p)$ cross sections [61].

As in every electron scattering experiment, radiative corrections had to be taken into account. These corrections are of two kinds. They may come first from bremsstrahlung and multiple scattering in the target liquid, in the windows of the spectrometers, and the walls of the cryotarget (external corrections). These corrections depend on the target thickness and induce energy losses which modify the kinematics of the vertex. They may as well originate from the renormalization of quantum electrodynamics vertices and propagators or from the emission of real photons by the incident (the outgoing) electron in the electromagnetic field of the target nucleus (internal corrections, which do not depend on the target thickness). The former processes cause no change in the kinematics at the vertex whereas the second do. All these processes have two effects on the experimental data: They diminish the counting rate and they create a tail in the missing energy spectrum of the $(e,e'p)$ events (see in Fig. 1 the radiative tail on the right of the 2BBU peak). We have adapted the (e,e') formulas of [62] to the case of $(e,e'p)$ reactions [59]. The radiative corrections amount to around 30% for our chosen integration interval of the counting rates of 4 MeV in missing energy on the right of the 2BBU peak.

C. Accuracy of the experiment

The statistical precision of our cross-section data was better than 1% (except for the p_r=150 MeV/c points, whose statistical precision was 2% or 3%). Data acquisition times were between a few minutes and 24 h.

The main systematic uncertainties of our measurements came from the beam charge, the detector (spectrometer) acceptance, the deuterium target thickness, the intrinsic detector efficiencies, and, as discussed in Sec. III A, the accuracy in determining p_r, the recoil momentum. The absolute uncertainty in the beam energy had been measured previously to be approximately 200 keV [63] and could be neglected.

We distinguish *differential* from *normalization* errors: *Differential* errors influenced the forward and the backward measurements differently and affected the coincidence cross-section ratio $\sigma^{\rm FW}_{(e,e'p)}/\sigma^{\rm BW}_{(e,e'p)}$. *Normalization* errors influenced the measurements of $\sigma^{\rm FW}_{(e,e'p)}$ and $\sigma^{\rm BW}_{(e,e'p)}$ proportionally. They led to an absolute normalization error in the experimental cross sections.

The *differential* errors reflected *instabilities* in the beam charge measurement, in the detector efficiencies, and in the target density. It also included the uncertainties in the recoil momentum. The errors in the *absolute* detector efficiencies and the *absolute* value of the target density affected $\sigma_{(e,e'p)}$ proportionally at all angles and energies and contribute to the error in the overall *normalization* of the cross sections.

Three independent devices were used to measure the beam charge; two were nonintercepting ferrite torroids upstream of the target. The third was a downstream beam stopping Faraday cup, located in a shielded area behind HE1. A systematic and constant difference of 0.5% was observed between the beam charge measured by the torroids and that measured with the Faraday cup. This contributed a normalization error of 0.5%, but no differential error to the cross sections.

With the method described in Sec. III A, the uncertainties in recoil momenta were found to be 0.5 MeV/c. This led to a 1% uncertainty in the cross section at low recoil momenta ($<$ 50 MeV/c) and a 2% uncertainty at higher recoil momenta.

During the experiment, particle detection occurred over the full extent of the focal planes of both spectrometers, and the coincidence events extended over a phase volume formed by the vector momenta of the coincidence electrons and protons. This phase volume, otherwise called the experimental acceptance, corresponded to an interval in recoil momentum of between 50 and 100 MeV/c. In this interval, the $(e,e'p)$ cross section varies nonlinearly over an order of magnitude [Eq. (8)]. Moreover, the solid angles defined by the spectrometer geometry depended on the position of the $(e,e'p)$ reaction vertex along the beam axis [61,64]. This dependence also had to be taken into account. These two finite geometry complications led us to use a Monte Carlo calculation to extract the $(e,e'p)$ cross sections from the raw data [61,64]. This calculation integrated a deuteron spectral function based on experimental data from [60,65] over the experimental acceptance of the 600 and the 900 spectrometers and over the target dimensions. It took account of particle energy losses. These calculations were calibrated, together with the target thickness and the detection efficiencies, in both spectrometers with the measurements of elastic electron-proton and electron-deuteron cross sections. Comparing the results of the Monte Carlo program for these elastic reactions

(which incorporated the electromagnetic proton [66] and deuteron [63] form factors, established to $\simeq$1%) with our measured counting rates, we found agreement on the average to within 0.5%, for both spectrometers, with variations of 1% (statistic plus systematic) about this value. The combined contribution of the uncertainties due to the experimental acceptance, the target density, the efficiencies of the 600 and the 900 spectrometers, and the beam charge measurement to the *differential* and *normalization* errors came to 1% and 0.5%, respectively. A further check on the consistency of our analysis was provided by the variation of the counting rates across the experimental phase space, which was accurately reproduced.

After the deuterium runs were over, we measured $(e,e'p)$ cross sections on hydrogen with a target full of liquid hydrogen. In this case, the electron-proton coincidences came from the elastic scattering of electrons by free protons, and the counting rates had to yield the elastic electron-proton cross section. Because of the complete correlation between the electron and the proton scattering angles, the coincidence solid angle was given by the electron solid angle *conditioned* by the presence of a proton in the 900 spectrometer. To properly compute this solid angle, we ran the same Monte Carlo simulation used to extract the ^{2}H$(e,e'p)$ cross sections. This allowed us to take into account the effect of Coulomb multiple scattering (CMS) on the coincidence counting rates. CMS has a strong effect on the ^{1}H$(e,e'p)$ scattering since, as the scattering angles are completely correlated, CMS can only destroy this correlation and cause a loss of true events. The influence of CMS on the ^{2}H$(e,e'p)$ scattering is less important. In fact, the momentum distribution of the proton inside the nucleus induces a proton angular distribution of finite width around the direction of the exchanged photon. This distribution is only slightly deformed by CMS, in contrast to the ^{1}H$(e,e'p)$ case. The hydrogen reaction is therefore more sensitive to CMS than the deuterium one [61].

We found a discrepancy between the experimental ^{1}H$(e,e'p)$ counting rates and those computed by the Monte Carlo program of 3% at forward angles and 4% at backward angles. This 1% difference was included in calculating the *differential* error. Considering the larger sensitivity of ^{1}H$(e,e'p)$ to CMS relative to ^{2}H$(e,e'p)$, we decided that instead of applying a renormalization factor to our measured ^{2}H$(e,e'p)$ cross sections, we enlarged our *normalization* error bars of 3% on both $\sigma^{\rm FW}_{(e,e'p)}$ and $\sigma^{\rm BW}_{(e,e'p)}$, that is to say, on the separated structure functions.

The total *differential* error on the experimental cross section then became 2.0% for small recoil momentum kinematics and 2.6% for recoil momentum above 50 MeV/c.

The total *normalization* error on the structure functions was the quadratic sum comprising a 3% uncertainty due to the results of the ^{1}H$(e,e'p)$ measurements, a 0.5% uncertainty on the beam charge measurement, detection efficiencies, etc. (see above), and the *differential* error listed above, amplified in the separation procedure.

The overall error on the separated spectral functions varied between 3% and 6% for $S_T^{\rm expt}$ and between 4% and 11% for $S_L^{\rm expt}$, and reflected the amplification factor cited above.

D. Kinematics

The aim of the experiment was to test our understanding of the $(e,e'p)$ reaction in the QE region by separating the longitudinal, transverse, and TL interference structure functions of the ^{2}H$(e,e'p)$ cross section. The "QE region" means that the energy transferred to the nucleus was near the peak of the inclusive reaction, viz., $\omega \approx \omega_{\rm QE} = Q^2/2M_p$. Our kinematics encompassed as wide a range of momentum transfer and recoil momenta as possible with our experimental setup and were chosen to investigate the following features of the reaction: the q dependence of σ_L and σ_T at p_r=20 and 100 MeV/c, the p_r dependences of σ_L, σ_T, and σ_{TL} at q=400 MeV/c, and the p_r dependence of σ_T at high (>0.8 GeV/c) momentum transfer.

The q dependence measurements were made in aligned kinematics ($\theta_{p'q}$=0). σ_L and σ_T and hence $S_L^{\rm expt}$ and $S_T^{\rm expt}$ were studied for 200 MeV/c < q < 670 MeV/c. Also measured were $S_L^{\rm expt}$ and $S_T^{\rm expt}$ at q = 650 MeV/c and p_r= 150 MeV/c; no q dependence could be measured at this relatively high value of the recoil momentum. For p_r = 100 MeV/c, the cross sections were measured in both parallel (where $\omega < \omega_{\rm QE}$) and antiparallel (where $\omega > \omega_{\rm QE}$) kinematics. One expects greater contributions from mesonic and isobar effects in the latter case than in the former. Tables I–IV describe these kinematics in detail.

TABLE I. Parallel kinematics at p_r = 20 MeV/c.

Kinematics	e (MeV)	e' (MeV)	$\theta_{e'}$ (deg)	p' (MeV/c)	$\theta_{p'}$ (deg)	q (MeV/c)	ω (MeV)
1	529.7	486.4	34.00	280	65.06	300	43.3
2	186.2	142.9	131.02	280	21.06	300	43.3
3	669.7	593.2	36.29	380	61.39	400	76.5
4	259.7	183.2	128.33	380	21.06	400	76.5
5	669.7	551.6	47.12	480	53.94	500	118.1
6	338.6	220.5	125.46	480	21.06	500	118.1
7	669.7	502.5	59.56	580	46.22	600	167.2
8	422.7	255.5	122.47	580	21.06	600	167.2
9	669.7	464.1	69.77	650	40.54	670	205.6
10	484.5	278.9	120.32	650	21.06	670	205.6

TABLE II. Parallel kinematics at $p_r = 100$ MeV/c.

Kinematics	e (MeV)	e' (MeV)	$\theta_{e'}$ (deg)	p' (MeV/c)	$\theta_{p'}$ (deg)	q (MeV/c)	ω (MeV)
11	669.7	615.4	36.00	300	64.60	400	54.3
12	246.2	191.9	131.49	300	21.06	400	54.3
13	669.7	580.5	46.47	400	57.33	500	89.2
14	320.7	231.5	129.08	400	21.06	500	89.2
15	669.7	537.3	58.39	500	49.70	600	132.4
16	400.5	268.1	126.47	500	21.06	600	132.4
17	669.7	522.6	65.42	570	45.18	670	167.2
18	459.4	292.3	124.56	570	21.06	670	167.2

TABLE III. Parallel kinematics at $p_r = 150$ MeV/c.

Kinematics	e (MeV)	e' (MeV)	$\theta_{e'}$ (deg)	p' (MeV/c)	$\theta_{p'}$ (deg)	q (MeV/c)	ω (MeV)
19	689.7	550.7	62.02	500	48.43	650	139.0
20	431.1	292.1	126.91	500	21.06	650	139.0

TABLE IV. Antiparallel kinematics at $p_r = 100$ MeV/c.

Kinematics	e (MeV)	e' (MeV)	$\theta_{e'}$ (deg)	p' (MeV/c)	$\theta_{p'}$ (deg)	q (MeV/c)	ω (MeV)
21	356.7	302.4	34.08	300	57.91	200	54.3
22	140.0	85.7	122.99	300	21.06	200	54.3
23	535.7	446.5	34.06	400	56.45	300	89.2
24	215.0	125.8	121.05	400	21.06	300	89.2
25	669.7	537.3	36.68	500	53.35	400	132.4
26	295.7	163.3	118.35	500	21.06	400	132.4
27	669.7	486.7	48.10	600	46.43	500	183.0
28	381.7	198.7	115.30	600	21.06	500	183.0

TABLE V. Orthogonal kinematics at $q = 400$ MeV/c.

Kinematics	e (MeV)	e' (MeV)	$\theta_{e'}$ (deg)	p' (MeV/c)	$\theta_{p'}$ (deg)	ω (MeV)	p_r (MeV/c)	$\theta_{p'q}$ (deg)	ϕ (rad)
29	669.7	583.2	36.41	403.1	52.82	86.5	50	7.125	0
30	669.7	583.2	36.41	403.1	67.07	86.5	50	7.125	π
31	259.1	172.6	134.87	403.1	24.93	86.5	50	7.125	π
32	669.7	575.6	36.49	412.3	44.81	94.1	100	14.04	0
33	669.7	575.6	36.49	412.3	72.88	94.1	100	14.04	π
34	262.7	168.6	134.87	412.3	31.42	94.1	100	14.04	π
35	669.7	562.9	36.59	427.2	36.47	106.8	150	20.56	0
36	669.7	562.9	36.59	427.2	77.58	106.8	150	20.56	π
37	268.8	162.1	134.87	427.2	37.24	106.8	150	20.56	π

TABLE VI. "High q" parallel kinematics.

Kinematics	e (MeV)	e' (MeV)	$\theta_{e'}$ (deg)	p' (MeV/c)	$\theta_{p'}$ (deg)	q (MeV/c)	ω (MeV)	p_r (MeV/c)
38	628.7	328.3	115.46	805	21.06	825	300.4	20
39	616.2	334.0	117.41	775	21.06	825	282.2	50
40	597.8	342.8	120.14	725	21.06	825	255.0	100
41	687.5	372.2	117.35	820	21.06	920	315.3	100
42	582.4	350.8	122.31	675	21.06	825	231.6	150

A stringent test of $(e,e'p)$ reaction models is provided by the TL interference structure function σ_{TL}, which can only be determined in nonaligned kinematics. In such kinematics (in plane), it is not possible to isolate σ_L; along with σ_T and σ_{TL}, only the structure function combination $\sigma_L + \sigma_{TT}$ can be determined. Fixing the momentum transfer at q=400 MeV/c, $\sigma_L + \sigma_{TT}$, σ_T, and σ_{TL} were obtained at recoil momenta of 50, 100, and 150 MeV/c (see Table V). Since σ_{TT} was at most 10% of σ_L, it could be reliably subtracted from $\sigma_L + \sigma_{TT}$ to obtain σ_L. For this purpose, σ_{TT} was calculated using the PWIA; reaction mechanisms not included in the PWIA modify the transverse structure function σ_T (and presumably σ_{TT}) by at most 20%. This implies an error in our method of subtracting σ_{TT} of at most 2% on σ_L.

Our "high q" measurements corresponded to momentum transfers greater than 800 MeV/c and utilized parallel kinematics. To reach these momentum transfers, the electrons were detected at backward angles (see Table VI) where the cross sections were mainly transverse, the longitudinal component making at most a 10% contribution. We therefore needed only to estimate σ_L to determine a reliable value of σ_T. Since the ejected protons had kinetic energies between 200 and 300 MeV, where the proton-neutron cross section has a minimum, rescattering effects should have been less important than at lower proton energies. Moreover, $\omega < \omega_{QE}$, so that mesonic and isobar effects were also minimized. These features suggest that PWIA calculations may be relatively successful in reproducing our high q measurements.

IV. RESULTS

A. Comparison with nonrelativistic models

We have plotted the experimental momentum distributions as functions of q for two values of p_r, 20 MeV/c in Fig. 2, 100 MeV/c in Fig. 3 (parallel kinematics—cf. also Tables VII–XII), and Fig. 4 (antiparallel kinematics). Differences in the q dependences of $S_L^{\rm expt}$ and $S_T^{\rm expt}$ are apparent: $S_L^{\rm expt}$ increases with q at low q, whereas $S_T^{\rm expt}$ is essentially constant with q in parallel kinematics (Figs. 2 and 3). The q dependences of both $S_L^{\rm expt}$ and $S_T^{\rm expt}$ for p_r=100 MeV/c differ markedly in parallel and antiparallel kinematics (Figs. 3 and 4). For q >500 MeV/c, $S_L^{\rm expt} \equiv S_L^{\rm expt}$ at p_r= 100 MeV/c; $S_L^{\rm expt}$ is about 10% smaller than $S_T^{\rm expt}$ at p_r=20 MeV/c.

The q dependences of $S_L^{\rm expt}$ and $S_T^{\rm expt}$ clearly show that in our kinematics, processes extrinsic to the PWIA play an important role in the ^{2}H$(e,e'p)$ reaction and act differently between parallel and antiparallel kinematics.

We have compared our data to model calculations of Arenhövel and co-workers [67–69] (dash-dotted curve in Figs. 2–6), Laget [70,71] (long-dashed curve), and Mosconi and co-workers [72–74] (dash-double-dotted curve). To make the comparison valid, we have divided their structure functions by the same elementary cc1 structure functions of de Forest used to form our experimental spectral functions. The comparison is then free of

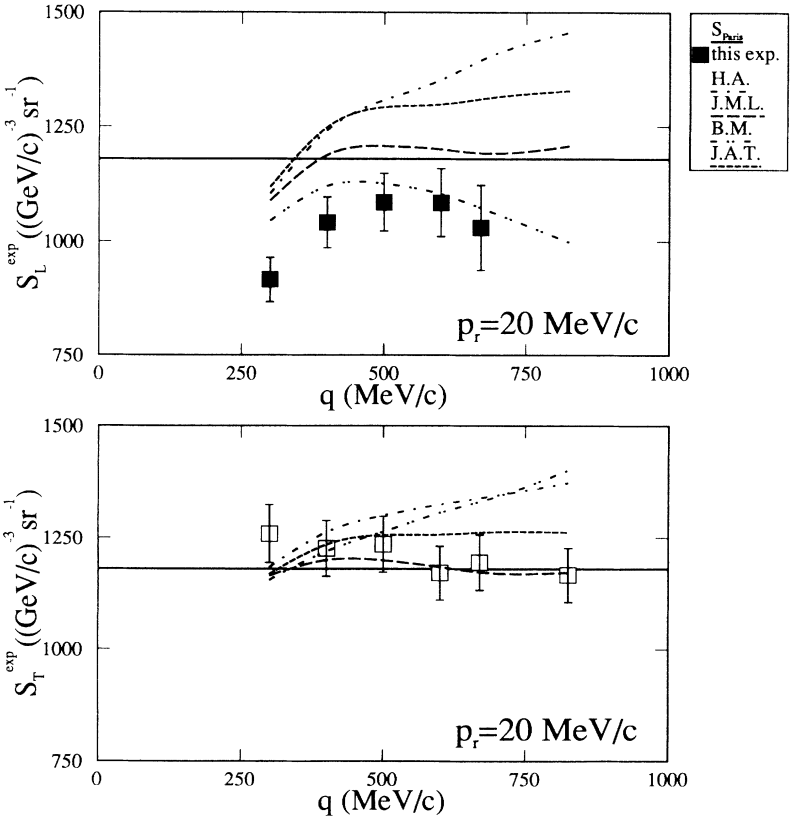

FIG. 2. $S_L^{\rm expt}$ and $S_T^{\rm expt}$ for p_r=20 MeV/c as functions of q. The legend of the curves is the following: The solid line ($S_{\rm Paris}$) is the proton momentum distribution given by the ^{2}H wave function computed with the Paris potential and extracted from $(e,e'p)$ cross sections with the plane wave impulse approximation (PWIA); the dash-dotted curve is the calculation from Arenhövel and co-workers (H.A.), the long-dashed curve is the calculation from Laget (J.M.L.), the dash-double-dotted curve is the calculation from Mosconi and co-workers (B.M.), and the dashed curve is the calculation from Hummel and Tjon (J.A.T.).

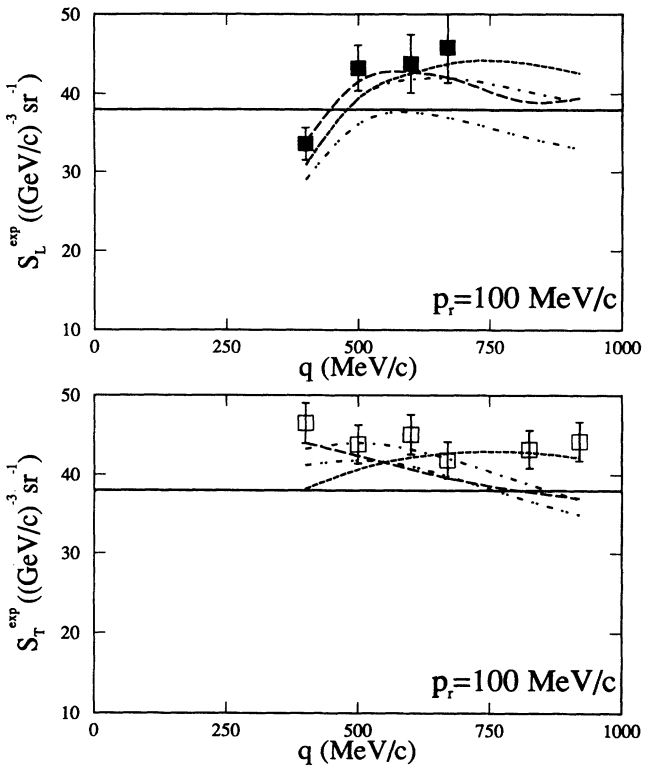

FIG. 3. S_L^{expt} and S_T^{expt} for p_r=100 MeV/c in parallel kinematics as functions of q. The legend of the curves is the same as in Fig. 2.

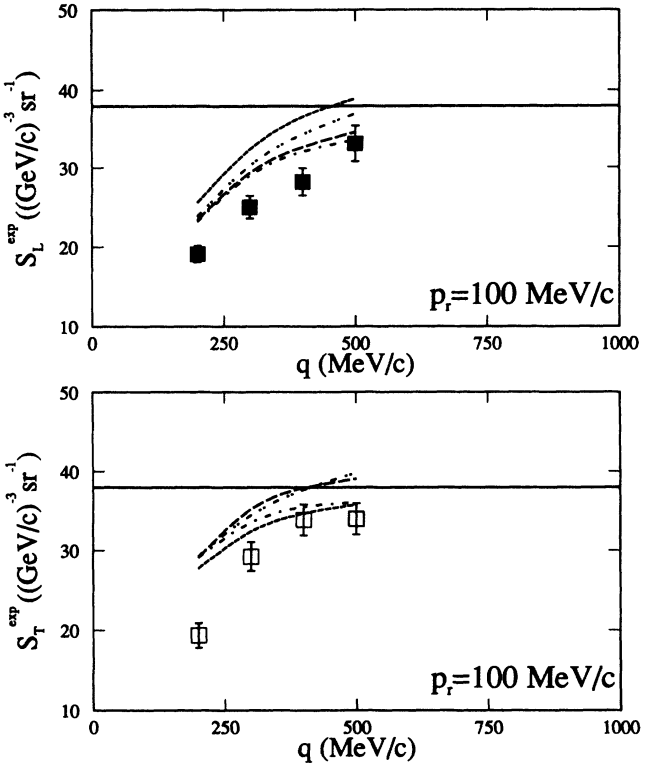

FIG. 4. S_L^{expt} and S_T^{expt} for p_r=100 MeV/c in antiparallel kinematics as functions of q. The legend of the curves is the same as in Fig. 2.

any model dependence, other than the assumption of the one-photon-exchange Born approximation; it is entirely equivalent to a comparison of the structure functions. The model calculations all use a nonrelativistic reduction, in terms of power of q/M_p of the electromagnetic current and density operators. They all incorporate processes extrinsic to the PWIA such as final state interactions (FSI's), computed by solving the Schrödinger equation (or the Lippmann-Schwinger equation in the momentum space) for the unbound proton+neutron system. Meson

TABLE VII. Results for the p_r = 20 MeV/c parallel kinematics. The first error is the statistical one; the second is the systematical one. The momentum distributions are given in (GeV/c)$^{-3}$ sr^{-1}.

Kinematics	$d^5\sigma/de'd\Omega_{e'}d\Omega_{p'}$ (nb/MeV sr^2)	S^{expt}	ε	S_L^{expt}	S_T^{expt}
1	436	968.4	0.84	916	1259
	±3.7±12.2	±8.4±22		±19±49	±25±65
2	21.3	1169	0.09		
	±0.18±0.47	±9.9±26			
3	259	1102	0.82	1041	1226
	±2.2±5.7	±9.4±24		±22±56	±24±63
4	17.6	1202	0.10		
	±0.15±0.39	±10±27			
5	98.6	1158	0.71	1086	1235
	±0.84±2.2	±9.8±25		±24±63	±24±63
6	13.9	1228	0.11		
	±0.12±0.31	±10±27			
7	38.6	1143	0.58	1085	1171
	±0.33±0.85	±9.7±25		±29±74	±23±60
8	9.95	1176	0.12		
	±0.085±0.22	±10±26			
9	21.2	1151	0.48	1030	1195
	±0.18±0.47	±9.8±25		±36±96	±24±62
10	8.16	1193	0.13		
	±0.069±0.18	±10±26			

TABLE VIII. Results for the p_r = 100 MeV/c parallel kinematics.

Kinematics	$d^5\sigma/de'd\Omega_{e'}d\Omega_{p'}$ (nb/MeV sr^2)	S^{expt}	ε	S_L^{expt}	S_T^{expt}
11	7.27	37.9	0.82	33.4	48.3
	±0.062±0.20	±0.32±1.1		±0.6±2.1	±0.8±2.5
12	0.547	45.3	0.09		
	±0.0046±0.015	±0.38±1.3			
13	3.30	44.1	0.72	43.0	45.5
	±0.028±0.092	±0.37±1.2		±0.9±2.9	±0.7±2.4
14	0.441	45.1	0.10		
	±0.0037±0.012	±0.38±1.3			
15	1.41	45.2	0.60	43.3	46.7
	±0.012±0.039	±0.38±1.3		±1.1±3.7	±0.8±2.5
16	0.347	46.3	0.11		
	±0.0029±0.0097	±0.39±1.3			
17	0.831	44.0	0.53	45.3	43.3
	±0.007±0.023	±0.37±1.2		±1.3±4.4	±0.7±2.3
18	0.265	43.5	0.11		
	±0.0022±0.0074	±0.37±1.2			

exchange currents (MEC's) and nucleonic resonance excitations are included as two-body current operators.

These calculations have the following specific features.

(1) Arenhövel and co-workers perform a completely nonrelativistic calculation, except for the kinematics. The T matrix involved in the cross section is developed in electric and magnetic multipoles and the proton-neutron rescattering is included in these multipoles up to an order $L_{\max}$=6. Plane wave terms are used for higher order multipoles. MEC's are computed consistent with the nucleon-nucleon potential used for the deuteron wave function and nucleonic resonances are introduced via the addition of supplementary currents: $N\Delta$, $\Delta\Delta$, $N'N$ terms.

(2) Laget introduces corrections of order $(q/M_p)^2$ and $(q/M_p)^3$ (*relativistic corrections*) in the nonrelativistic reduction of the electromagnetic one-body current. The elementary reaction amplitude is developed as a sum of elementary proton-neutron amplitudes and includes charge exchange, rescattering, meson exchange, and virtual resonance excitation diagrams.

(3) Mosconi and co-workers also employ a multipole expansion treatment, but which differs from that of Arenhövel and co-workers in including relativistic corrections to the nuclear current of order $(q/M_p)^2$ and $(q/M_p)^3$ to the nuclear current. These terms reflect Darwin-Foldy and spin-orbit corrections in the nucleon one-body current, relativistic effects from the distortion of the intrinsic nuclear wave function by the nuclear motion [75,76] and pionic corrections to the charge density (in the electric multipoles up to $L_{\max}$=6) using Siegert's theorem [77].

These models use the same deuteron wave function, given by the Paris nucleon-nucleon potential [78–80]. This means that the differences between the various spectral functions extracted from the models reflect only differences in the computation of reaction mechanism effects. It is to be noted that the models of Arenhövel and co-workers and of Laget successfully describe the inclusive ^{2}H(e,e') quasielastic data of Bates [16,17].

Figures 2–4 show that the models reproduce the data reasonably well, at least at p_r=100 MeV/c in parallel kinematics (Fig. 3): The dip of S_L^{expt} at low q as well as the equality of S_L^{expt} and S_T^{expt} above q = 500 MeV/c is well reproduced. The calculations confirm that the contribution of MEC's is small in our kinematics, even in the antiparallel configuration (Fig. 4, $\omega > \omega_{\text{QE}}$) where they contribute only $\sim$ 10% of the transverse structure function. Rescattering effects in the final state explain most of the difference between the parallel and antiparallel kinematics and seem to be therefore well characterized.

What is not reproduced by these calculations is the low q value of S_L^{expt} at p_r= 20 MeV/c (Fig. 2, upper) and p_r=100 MeV/c in antiparallel kinematics (Fig. 4, upper) and the value of S_T^{expt} at $q > 800$ MeV/c (Fig. 3, lower; note that in this figure four calculations are drawn; the three discussed here lie above the data). The situation can be summarized by saying that there is rough agreement between these calculations and the experiment at the 10% level, but none of these calculations describes the data consistently to this level of accuracy.

In Fig. 5 we have plotted the ratios $S_\alpha^{\text{expt}}/S_{\text{Paris}}$ (α =

TABLE IX. Results for the p_r = 150 MeV/c parallel kinematics.

Kinematics	$d^5\sigma/de'd\Omega_{e'}d\Omega_{p'}$ (nb/MeV sr^2)	S^{expt}	ε	S_L^{expt}	S_T^{expt}
19	0.192	9.21	0.57	7.68	9.86
	±0.0041±0.0041	±0.2±0.2		±0.83±0.83	±0.53±0.53
20	0.0593	9.94	0.11		
	±0.0013±0.0013	±0.2±0.2			

TABLE X. Results for the p_r = 100 MeV/c antiparallel kinematics.

Kinematics	$d^5\sigma/de'd\Omega_{e'}d\Omega_{p'}$ (nb/MeV sr^2)	S^{expt}	ε	S_L^{expt}	S_T^{expt}
21	21.2	18.9	0.83	19.12	19.35
	±0.18±0.59	±0.16±0.52		±0.3±1.0	±0.5±1.5
22	0.653	18.6	0.12		
	±0.0055±0.018	±0.16±0.52			
23	14.6	25.5	0.83	24.99	29.23
	±0.12±0.41	±0.22±0.75		±0.4±1.4	±0.5±1.8
24	0.656	26.7	0.13		
	±0.0056±0.018	±0.23±0.74			
25	8.28	29.6	0.80	28.20	33.85
	±0.070±0.23	±0.25±0.82		±0.5±1.7	±0.6±2.0
26	0.575	31.3	0.14		
	±0.0049±0.016	±0.27±0.88			
27	3.12	33.0	0.69	33.10	33.96
	±0.026±0.087	±0.28±0.94		±0.7±2.3	±0.6±2.0
28	0.453	32.83	0.15		
	±0.0038±0.013	±0.28±0.96			

L, T, TL) as functions of p_r (S_{Paris} is the proton momentum distribution given by the Paris potential). These ratios are convenient to consider since they vary at most by 50% between p_r=0 and 150 MeV/c, while S_{Paris} falls by two orders of magnitude in this interval. We see in Fig. 5 that $S_L^{\text{expt}}/S_{\text{Paris}}$ decreases more rapidly with increasing p_r than do $S_T^{\text{expt}}/S_{\text{Paris}}$ and $S_{TL}^{\text{expt}}/S_{\text{Paris}}$. These features are quite well reproduced by the models. However, we note that the longitudinal structure function is better described at p_r=150 MeV/c by the curves of Laget and Mosconi and co-workers than by Arenhövel and co-workers. This would appear to support the argument of Mosconi and Ricci concerning the relatively high sensitivity of σ_L and σ_{TL} to relativistic corrections [74]. Unfortunately, σ_{TL} is only well reproduced by the nonrelativistic curve of Arenhövel and co-workers. Relativistic corrections appear to raise the theoretical TL curve, as has been shown by Laget; the relativistic correction terms $(q/M_p)^2$ and $(q/M_p)^3$ in the electromagnetic operator worsen his agreement with our σ_{TL} data by increasing its prediction for this structure function by 30% [81].

Figure 6 shows our data for $S_T^{\text{expt}}/S_{\text{Paris}}$ as a function of p_r at high q (>800 MeV/c). None of the calculations we have been discussing agree well with the data.

B. Relativistic effects

We have seen that the relativistic corrections of order $(q/M_p)^2$ and $(q/M_p)^3$ to the electromagnetic nuclear current are ambiguous. On the one hand, they appear to increase the disagreement between the complete calculation of Laget and our TL interference structure function

TABLE XI. Results for the q = 400 MeV/c orthogonal kinematics.

Kinematics	$d^5\sigma/de'd\Omega_{e'}d\Omega_{p'}$ (nb/MeV sr^2)	S^{expt}	ε	S_L^{expt}	S_T^{expt}	S_{TL}^{expt}
29	65.2	296.2	0.81	278.9	326.7	276.4
	±0.55±1.8	±2.5±8.3		±5.3±17.7	±6.7±22.2	±8.9±29.8
30	77.8	290.9	0.81			
	±0.67±2.2	±2.5±8.1				
31	4.59	314.3	0.08			
	±0.039±0.13	±2.7±8.8				
32	5.30	26.7	0.81	25.3	33.6	30.3
	±0.045±0.15	±0.2±0.7		±0.5±1.6	±0.7±2.3	±0.7±2.2
33	8.55	28.4	0.81			
	±0.073±0.24	±0.2±0.8				
34	0.498	31.9	0.08			
	±0.0042±0.014	±0.3±0.9				
35	0.642	3.59	0.81	3.39	6.06	5.63
	±0.018±0.018	±0.1±0.1		±0.2±0.2	±0.4±0.4	±0.4±0.4
36	1.52	4.55	0.81			
	±0.043±0.043	±0.1±0.1				
37	0.0936	5.61	0.07			
	±0.0026±0.0026	±0.2±0.2				

TABLE XII. Results for the "high q" parallel kinematics.

Kinematics	$d^5\sigma/de'd\Omega_{e'}d\Omega_{p'}$ (nb/MeV sr^2)	S_T^{expt}	ϵ
38	4.97	1167	0.13
	±0.042±0.13	±9.9±33	
39	1.49	366.7	0.14
	±0.013±0.042	±3.1±10	
40	0.169	43.2	0.13
	±0.0029±0.0056	±0.8±1.4	
41	0.124	44.2	0.13
	±0.0042±0.0042	±1.4±1.4	
42	0.0334	9.19	0.12
	±0.0114±0.0114	±0.3±0.3	

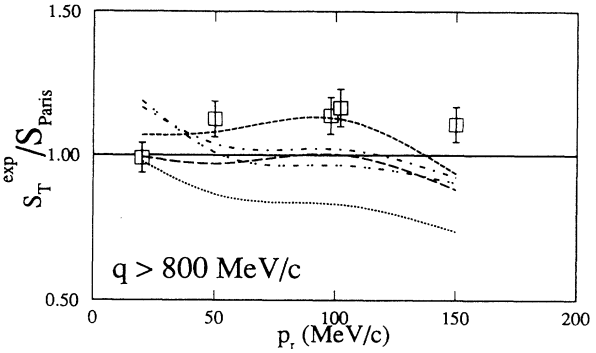

FIG. 6. S_T^{expt} and S_{Paris} for q=400 MeV/c in antiparallel kinematics as functions of p_r. The legend of the curves is the same as in Fig. 5.

data; on the other hand, they are needed in principle to account for the first order relativistic effects in the reaction.

Beck and Arenhövel have added relativistic corrections to their completely nonrelativistic calculation [82]. The calculation includes correction terms of order $(q/M_p)^2$ and $(q/M_p)^3$ consistently in both the electromagnetic current and the deuteron wave function. The corrections in the deuteron wave function relate to the modification of the intrinsic wave function in the nucleonic rest frame and the Lorentz boost effect between this frame and the laboratory frame. We compare this model to our orthogonal kinematics data in Fig. 5 and to our high q data in Fig. 6. In both figures, the calculation is represented by the dotted curve. In Fig. 5, the S_L^{expt} data are in slightly better agreement with this curve than with the curve of the nonrelativistic calculation. In contrast, the S_{TL}^{expt} data point at p_r=100 MeV/c seems to agree less well with the relativistic curve. However, the most striking result, seen in Fig. 6, is the strong disagreement of the relativistic curve with our high q kinematics data.

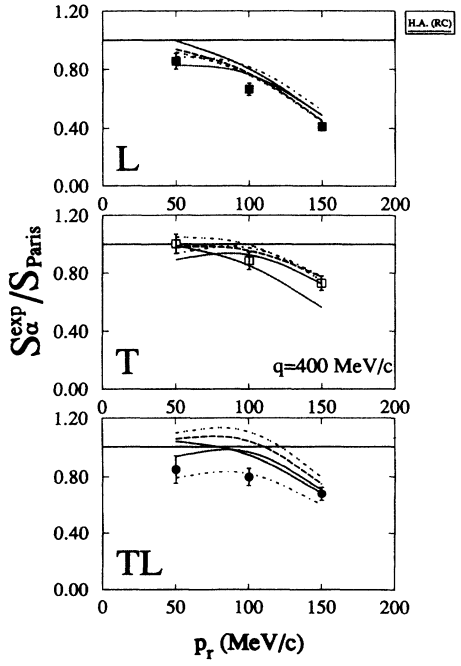

FIG. 5. $S_\alpha^{\text{expt}}/S_{\text{Paris}}$, $\alpha = L, T, TL$ for q = 400 MeV/c in orthogonal kinematics as functions of p_r. The legend of the curves is the same as in Fig. 2 except that the dotted curve is a calculation from Arenhövel and co-workers which includes relativistic corrections (H.A. RC).

What we can conclude, as far as these relativistic corrections are concerned, is not clear. The calculation of Beck and Arenhövel with relativistic corrections agrees neither with the calculations of Laget nor Mosconi and co-workers, both of whom include such corrections in the nuclear current. Furthermore, none of the relativistically corrected models are able to reproduce our data better than the completely nonrelativistic model of Beck and Arenhövel. These different calculations seem neither consistent with each other nor consistently adequate to describe our data.

To further probe the nature of relativistic effects, we have compared our data to a recent calculation by Hummel and Tjon [83]. This calculation is based on a fully covariant approach and uses quasipotential equations. These equations rely on a relativistic one-boson-exchange (OBE) potential with π, ρ, ϵ, ω, η, and δ terms. This model was used rather successfully to determine deuteron elastic form factors [84]. In view of our quasielastic kinematics and our relatively small momentum and energy transfers, MEC's and nucleonic negative energy state contributions were omitted in this calculation.

We have compared the Hummel-Tjon calculations (the short-dashed curve in the figures) to all our data. The small momentum transfer data serve to "calibrate" the calculations, since relativistic effects are presumably small there. The high momentum transfer data, where such effects ought to be appreciable, can serve to evaluate their importance.

We see in Figs. 2–6 that the Hummel-Tjon model is as successful as the others, the agreement with the data being of the order of 10%. As far as σ_{TL} is concerned, the Hummel-Tjon predictions lie between those of Laget and Mosconi and co-workers and our data.

The data for the high q (>800 MeV/c) kinematics would seem particularly relevant in evaluating the dif-

ferent models, since rescattering corrections are smaller. We see (Fig. 6) that the value of the ratio $S_T^{\rm expt}/S_{\rm Paris}$ as a function of p_r is closer to the calculation of Hummel and Tjon than to other calculations but the highest p_r point is not reproduced by Hummel and Tjon. This has to be put in parallel with the disagreement between our data and these calculations for the transverse structure function of the orthogonal kinematics (see Fig. 5) and may be due to MEC's, whose contribution increases as p_r increases, reaching a level of 20% of the PWIA value at p_r=150 MeV/c.

C. Comparison with other ^{2}H($e,e'p$) experiments

Previous ^{2}H($e,e'p$) experiments in the early 80s [60,65] measured cross sections (structure functions were not extracted) to test the general validity of the impulse approximation. The PWIA nucleon momentum density in deuterium was extracted directly from those cross sections. Recoil momenta were in the range $0 \leq p_r \leq 500$ MeV/c, with q varying inversely between 450 and 280 MeV/c. The experimental momentum distribution was found to be about 15% less than the Paris potential prediction at low recoil momenta ($p_r < 50$ MeV/c). Better agreement was obtained for higher momenta. At small recoil momenta in our present work, we too find (Fig. 2) that $S_L^{\rm expt}$ is less than the PWIA prediction, by 15–20 %. For the kinematics of the early Saclay work, the ϵ parameter was 0.6–0.7, values for which the longitudinal component of the cross section is large ($\epsilon\sigma_L/\sigma_T \sim 3$). It is not unreasonable to suggest therefore that the observed low values of the early measurements of $S^{\rm expt}$ had their origin in the low values of the longitudinal response $S_L^{\rm expt}$ (since $S_T^{\rm expt}$ agrees with the Paris potential value, it tends only to dilute the discrepancy observed in the earlier Saclay data).

More recently, ^{2}H($e,e'p$) measurements have been made at NIKHEF [35,36]. In aligned kinematics, longitudinal and transverse structure functions were determined for $40 < p_r < 110$ MeV/c and q varying from 260 to 500 MeV/c [35]. Most of these measurements were in the antiparallel configuration, where we have seen that $S_L^{\rm expt}$ and $S_T^{\rm expt}$ agree less with the theory. Other measurements were made in the nonaligned configuration to determine the TL interference structure functions [36].

TABLE XIII. Comparison between NIKHEF and Saclay data for the TL interference structure function. The quoted errors are statistical.

p_r (MeV/c)	Saclay (fm)	NIKHEF (fm)
50	0.267±0.069	0.465±0.16
100	0.0567±0.0042	0.064±0.024
150	0.0196±0.0014	0.017±0.024

The comparison between NIKHEF data and ours is shown in Fig. 7 (aligned kinematics) and in Table XIII (interference structure function). In Fig. 7, the comparison is made in terms of the parameter R_G [35]:

$$R_G = \sqrt{\frac{2M_p^2}{Q^2}\frac{f_T}{f_L}} = \sqrt{\frac{2M_p^2}{\mathbf{q}_{\rm c.m.}^2}\frac{\sigma_T}{\sigma_L}}, \tag{10}$$

where the f_α, $\alpha = L$, T, TL, TT are defined in [67,68] and $\mathbf{q}_{\rm c.m.}$ is the three-momentum transfer in the center-of-mass frame of the virtual photon-deuteron system. In the PWIA, R_G reduces, apart from off-shell effects, to the proton form factor ratio $G_M^p/G_E^p = 2.79$. We can see in Fig. 7 that the Saclay values (squares) and NIKHEF values (solid circles) largely overlap and have mean values slightly above the PWIA value.

In Table XIII, we show f_{TL} for three values of the recoil momentum: 50, 100, and 150 MeV/c, extracted from the data of Saclay and NIKHEF. The NIKHEF values at these momenta were obtained by interpolating between the values given in [85] to the right value of the recoil momentum. The Saclay values were obtained by multiplying the experimentally determined TL structure functions by ratios of f_{TL} from Arenhövel and co-workers [82]

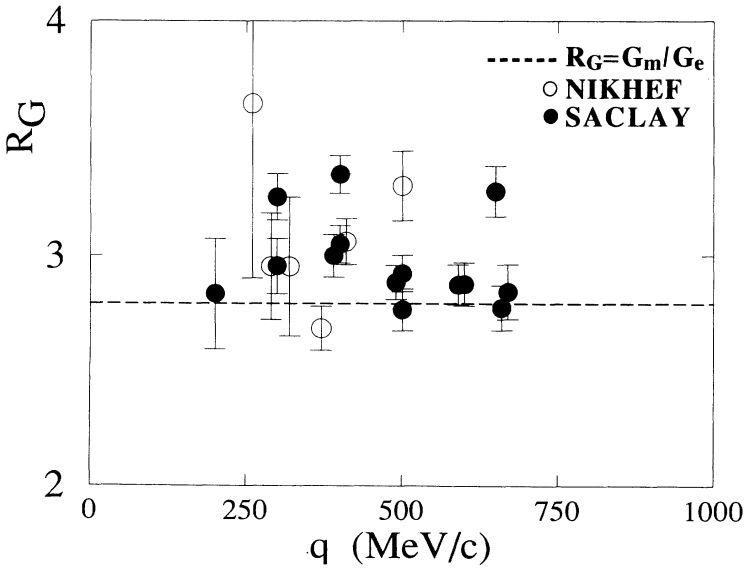

FIG. 7. Experimental data for $R_G = \sqrt{(2M_p^2/\mathbf{q}_{\rm c.m.}^2)/(\sigma_T/\sigma_L)}$ as measured at NIKHEF (solid circles) and Saclay (squares). $R_G = G_m/G_e \simeq 2.79$ is the value obtained in the PWIA with the approximation $Q^2 = \mathbf{q}_{\rm c.m.}^2$.

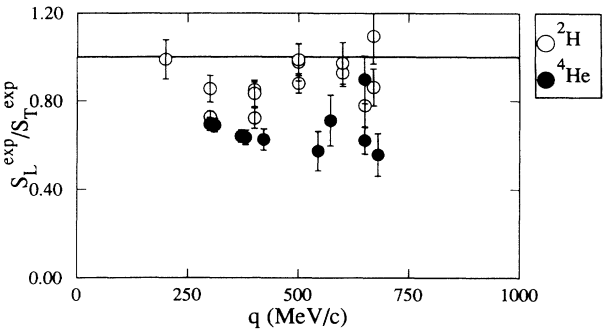

FIG. 8. The ratios $S_L^{\text{expt}}/S_T^{\text{expt}}$ for the reactions $^2\text{H}(e,e'p)$ and $^4\text{He}(e,e'p)^3\text{H}$ as functions of q (see [43]).

to adjust our values to the NIKHEF kinematics. These ratios were computed with both nonrelativistic and relativistic calculations described in Secs. IV A and IV B. The differences were of the order 5%. In Table XIII, we observe that the NIKHEF and Saclay data are in basic agreement. This is rather surprising since Saclay data are better described by the nonrelativistic calculation of Arenhövel and co-workers, whereas the NIKHEF data are said to be better described by the relativistic model of Hummel and Tjon. This confused situation will have to be clarified by new measurements at upcoming electron facilities. In any case, our attempts to compare the Saclay and NIKHEF data suffer from the amplification of the errors due to our interpolation of the NIKHEF data and the adjustments made to the Saclay data.

D. Comparison with ^{4}He

Longitudinal and transverse $(e,e'p)$ structure functions (in the two-body break-up channel) have now been determined at Saclay for ^{2}H, ^{3}He, and ^{4}He [42–46]. In Fig. 8 we show the q dependence of $S_L^{\text{expt}}/S_T^{\text{expt}}$ for ^{2}H (circles) and ^{4}He (solid circles) at recoil momenta ranging from 20 to 190 MeV/c. The line at $S_L^{\text{expt}}/S_T^{\text{expt}}=1$ is the PWIA value. We observe a marked difference between the two nuclei. For ^{2}H, $S_L^{\text{expt}}/S_T^{\text{expt}} \simeq 1$ for $q \geq 500$ MeV/c, similar to what has been measured in ^{3}He [44], whereas for ^{4}He, $S_L^{\text{expt}}/S_T^{\text{expt}} \simeq 0.65$ throughout the range of momentum transfer.

The distinct difference between these ratios for ^{2}H (and ^{3}He), on the one hand, and ^{4}He, on the other hand, can be attributed to non-PWIA effects, which are greater in ^{4}He than in ^{2}H and ^{3}He; attempts to compute these effects were only partially successful [42,43]. A similar behavior was observed in the ratios of the longitudinal and transverse response functions of the *inclusive* reaction on ^{2}H, ^{3}He, and ^{4}He [24], which suggests that the problems in adequately describing the inclusive and exclusive reactions are likely to have the same origin.

V. CONCLUSION

$^2\text{H}(e,e'p)$ cross sections have been measured at the linear electron accelerator of Saclay in order to separate the longitudinal, transverse, and interference (TL) structure functions of the reaction. From these structure functions, experimental spectral functions S_L^{expt}, S_T^{expt}, and S_{TL}^{expt} have been defined by dividing the $(e,e'p)$ structure functions by corresponding structure functions taken from the cc1 off-shell electron-proton cross section of de Forest.

Unlike the conclusions derived from the plane wave impulse approximation (PWIA), S_L^{expt} and S_T^{expt} differ in their momentum transfer (q) dependence. In particular, we find the following: S_L^{expt} and S_T^{expt} depend upon q below 500 MeV/c; no q dependence is evident above 500 MeV/c. S_L^{expt} can differ from S_T^{expt} by up to 10%, even at $q > 500$ MeV/c. The dependence of S_L^{expt} and S_T^{expt} on q differs for parallel ($\omega < \omega_{\text{QE}}$) and antiparallel ($\omega > \omega_{\text{QE}}$) kinematics.

The p_r dependences of the structure functions between 0 and 150 MeV/c also differ: At q= 400 MeV/c, S_L^{expt} falls more steeply with p_r than do S_T^{expt} or S_{TL}^{expt}. For q above 800 MeV/c, the p_r dependence of S_T^{expt} disagrees with the PWIA (Paris potential) prediction.

A comparison to various calculations has been made. Four are fundamentally nonrelativistic, employing the same NN (Paris) interaction but having different relativistic corrections in the electromagnetic operators and nuclear wave function; another is fully relativistic. The mean disagreement of the calculations with our S_L^{expt} and S_T^{expt} is at the level of 10% for $q < 700$ MeV/c; commensurate differences appear between the calculations. We can conclude that in this range of momentum and energy transfer, the basic quasielastic $(e,e'p)$ reaction mechanisms are, at the 10% level, adequately described.

It is difficult to characterize the relative success of the calculations. Our $q > 800$ MeV/c data are best described by a fully relativistic model of Hummel and Tjon, whereas the LT interference structure function data, said to be especially sensitive to relativistic corrections, are best fit by a completely nonrelativistic model of Arenhövel and co-workers [67–69]. A disconcerting feature is the spread of the calculations, about 25% for S_L^{expt} at p_r= 20 MeV/c and q= 825 MeV/c. It suggests that the nature of the relativistic corrections needs to be clarified, a task appropriate to facilities which can access higher momentum components of the nuclear wave function at higher momentum transfers.

If scattering from deuterium constitutes a standard to which calculations in more complex nuclei should be compared, we can at best expect agreement to within 10–15% between theory and experimental structure functions. From this point of view, it is not surprising that $(e,e'p)$ structure function data and (e,e') response function data on nuclei such as ^{4}He and ^{40}Ca (at least the data from Saclay in this last case, as previously mentioned), where the nuclear environment is more complex, are less well explained. From a purely experimental point of view, in the region $q < 700$ MeV/c and $p_r < 100$ MeV/c, the behavior of the longitudinal and transverse

structure functions in the transition from ^{2}H to ^{4}He and heavier targets is striking: $S_L^{\text{expt}}/S_T^{\text{expt}} = 0.65$ in ^{4}He, similar to what was measured in ^{40}Ca, whereas it is very close to unity in ^{2}H. The similarity of this ratio to what has been found in the ratio of the longitudinal and transverse scaling functions near the quasielastic peak lends credence to the notion that a key to understanding the inclusive channels lies in the behavior of the $(e,e'p)$ structure functions.

ACKNOWLEDGMENTS

We would like to thank J. M. Laget and B. Mosconi for their calculations and their useful comments on the comparison between our data and theory. J. A. Tjon provided us with his new calculations before publication and is gratefully acknowledged. The work of one of us (M.K.B.) was supported in part by the U.S. National Science Foundation under Contract No. PHY86-10493.

[1] V. Breton *et al.*, Phys. Rev. Lett. **66**, 572 (1991).
[2] E. J. Moniz, I. Sick, R. R. Whitney, J. R. Ficenec, R. D. Kephart, and W. P. Trower, Phys. Rev. Lett. **26**, 445 (1971).
[3] M. Gourdin, Nuovo Cimento **21**, 1094 (1961).
[4] R. Altemus, A. Cafolla, D. Day, J. S. McCarthy, R. R. Whitney, and J. E. Wise, Phys. Rev. Lett. **44**, 965 (1980).
[5] P. Barreau *et al.*, Nucl. Phys. **A358**, 287c (1981).
[6] P. Barreau *et al.*, Nucl. Phys. **A402**, 515 (1983).
[7] M. Deady, C. F. Williamson, J. Wong, P. D. Zimmermann, C. Blatchley, J. M. Finn, J. LeRose, P. Sioshansi, R. Altemus, J. S. McCarthy, and R. R. Whitney, Phys. Rev. C **28**, 631 (1983).
[8] M. Deady, C. F. Williamson, P. D. Zimmermann, R. Altemus, and R. R. Whitney, Phys. Rev. C **33**, 1897 (1986).
[9] J. M. Finn, R. W. Lourie, and B. H. Cottman, Phys. Rev. C **29**, 2230 (1984).
[10] A. Hotta, P. J. Ryan, H. Ogino, B. Parker, G. A. Peterson, and R. P. Singhal, Phys. Rev. C **30**, 87 (1984).
[11] Z. E. Meziani *et al.*, Phys. Rev. Lett. **52**, 2130 (1984).
[12] Z. E. Meziani *et al.*, Phys. Rev. Lett. **54**, 1233 (1985).
[13] Z. E. Meziani *et al.*, Nucl. Phys. **A446**, 113c (1985).
[14] C. Marchand, P. Barreau, M. Bernheim, P. Bradu, G. Fournier, Z. E. Meziani, J. Miller, J. Morgenstern, J. Picard, B. Saghaï, S. Turck-Chieze, and P. Vernin, Phys. Lett. **153B**, 29 (1985).
[15] K. Dow *et al.*, Phys. Rev. Lett. **61**, 1706 (1988).
[16] B. P. Quinn *et al.*, Phys. Rev. C **37**, 1609 (1988).
[17] S. A. Dytman, A. M. Bernstein, K. I. Blomqvist, T. J. Pavel, B. P. Quinn, R. Altemus, J. S. McCarthy, G. H. Mechtel, T. S. Ueng, and R. R. Whitney, Phys. Rev. C **38**, 800 (1988).
[18] K. F. von Reden *et al.*, Phys. Rev. C **41**, 1084 (1990).
[19] A. Zghiche, thèse, Université d' Orsay, France, 1989.
[20] J. F. Danel, thèse, Université d'Orsay, France, 1990.
[21] J. P. Chen *et al.*, Phys. Rev. Lett. **66**, 1283 (1991).
[22] Z. E. Meziani *et al.*, Phys. Rev. Lett. **69**, 41 (1992).
[23] T. C. Yates *et al.*, Phys. Lett. B **312**, 382 (1993).
[24] A. Zghiche *et al.*, Nucl. Phys. **A** (to be published).
[25] S. Fantoni and V. R. Pandharipande, Nucl. Phys. **A473**, 234 (1987).
[26] G. Co', K. F. Quader, R. D. Smith, and J. Wambach, Nucl. Phys. **A485**, 61 (1988).
[27] G. Do Dang and N. Van Giai, Phys. Rev. C **30**, 731 (1984).
[28] H. Kurasawa and T. Suzuki, Nucl. Phys. **A490**, 571 (1988).
[29] C. J. Horowitz and J. Piekarewicz, Phys. Rev. Lett. **62**, 391 (1989).
[30] J. V. Noble, Phys. Rev. Lett. **46**, 412 (1981).
[31] L. S. Celenza, A. Rosenthal, and C. M. Shakin, Phys. Rev. Lett. **53**, 892 (1985).
[32] L. S. Celenza, A. Harindranath, A. Rosenthal, and C. M. Shakin, Phys. Rev. C **31**, 946 (1985).
[33] L. S. Celenza, A. Harindranath, and C. M. Shakin, Phys. Rev. C **33**, 1012 (1986).
[34] P. J. Mulders, Phys. Rev. Lett. **54**, 2560 (1985); Phys. Rep. **185**, 83 (1990).
[35] M. van der Schaar *et al.*, Phys. Rev. Lett. **66**, 2855 (1991).
[36] M. van der Schaar *et al.*, Phys. Rev. Lett. **68**, 776 (1992).
[37] G. van der Steenhoven *et al.*, Phys. Rev. Lett. **58**, 1727 (1987).
[38] G. van der Steenhoven *et al.*, Phys. Rev. Lett. **57**, 182 (1986).
[39] P. E. Ulmer *et al.*, Phys. Rev. Lett. **59**, 2259 (1987).
[40] D. Reffay-Pikeroen *et al.*, Phys. Rev. Lett. **60**, 776 (1988).
[41] J. Morgenstern, Nucl. Phys. **A446**, 315c (1985).
[42] A. Magnon *et al.*, Phys. Lett. B **222**, 352 (1989).
[43] J. E. Ducret *et al.*, Nucl. Phys. **A556**, 373 (1993).
[44] L. Lakehal-Ayat *et al.*, in *Proceedings of the Fifth Workshop on Perspectives in Nuclear Physics at Intermediate Energies*, Trieste, Italy, edited by S. Boffi, C. Ciofi Degli Atti, and M. Giannini (World Scientific, Singapore, 1992), p. 218; L. Lakehal-Ayat, thèse, Université d'Orsay, France, 1991.
[45] L. Lakehal-Ayat *et al.*, Nucl. Phys. **A553**, 693c (1993).
[46] J. E. Ducret *et al.*, Nucl. Phys. **A553**, 697c (1993).
[47] G. F. Chew and G. C. Wick, Phys. Rev. **85**, 636 (1952).
[48] S. Frullani and J. Mougey, Adv. Nucl. Phys. **14**, 1 (1984).
[49] N. Dombey, Rev. Mod. Phys. **41**, 236 (1969).
[50] C. Giusti and F. D. Pacati, Nucl. Phys. **A473**, 717 (1987).
[51] M. Traini, S. Turck Chieze, and A. Zghiche, Phys. Rev. C **38**, 2799 (1988).
[52] M. N. Rosenbluth, Phys. Rev. **79**, 615 (1950).
[53] C. Papanicolas *et al.*, Nucl. Phys. **A497**, 509c (1989), and Bates proposals Nos. 87-07, 87-09, and 87-10.
[54] For a review on $(e,e'p)$ reaction mechanisms, see S. Frullani and J. Mougey, Adv. Nucl. Phys. **14**, 1 (1984) or H. Arenhövel, in *Modern Topics in Electron Scattering*, edited by B. Frois and I. Sick (World Scientific, Singa-

pore, 1991), and references therein.
[55] T. de Forest, Nucl. Phys. **A392**, 232 (1983).
[56] J. Mougey, thèse, Université d'Orsay, France, 1976.
[57] P. Leconte, thèse, Université d'Orsay, France, 1976.
[58] P. Leconte *et al.*, Nucl. Instrum. Methods **169**, 401 (1980).
[59] C. Marchand, thèse, Université d'Orsay, France, 1987.
[60] M. Bernheim *et al.*, Nucl. Phys. **A365**, 349 (1981).
[61] J. E. Ducret, thèse, Université d'Orsay, France, 1992.
[62] L. W. Mo and Y. S. Tsai, Rev. Mod. Phys. **41**, 205 (1969).
[63] S. Platchkov *et al.*, Nucl. Phys. **A584**, 343c (1990); private communication.
[64] J. M. Le Goff and P. Vernin, C.E.A. internal report, 1987.
[65] S. Turck-Chieze *et al.*, Phys. Lett. **142B**, 145 (1984).
[66] G. G. Simon *et al.*, Nucl. Phys. **A333**, 381 (1980).
[67] W. Fabian and H. Arenhövel, Nucl. Phys. **A258**, 461 (1976).
[68] W. Fabian and H. Arenhövel, Nucl. Phys. **A314**, 253 (1979).
[69] H. Arenhövel, W. Leidemann, and E.L. Tomusiak, Z. Phys. A **331**, 123 (1988).
[70] J. M. Laget, Can. J. Phys. **62**, 1046 (1984).
[71] J. M. Laget, Phys. Lett. B **199**, 493 (1987).
[72] A. Cambi, B. Mosconi, and P. Ricci, Phys. Rev. Lett. **48**, 462 (1982).
[73] A. Cambi, B. Mosconi, and P. Ricci, Phys. Rev. C **26**, 2358 (1982).
[74] B. Mosconi and P. Ricci, Nucl. Phys. **A517**, 483 (1990).
[75] R. A. Krajcik and L. L. Foldy, Phys. Rev. D **10**, 1777 (1974).
[76] J. L. Friar, Phys. Rev. C **12**, 696 (1975).
[77] J. L. Friar, Ann. Phys. (N.Y.) **104**, 380 (1977); Phys. Rev. C **22**, 796 (1980).
[78] M. Lacombe, B. Loiseau, J. M. Richard, R. Vinh Mau, P. Pirès, and R. de Tourreil, Phys. Rev. D **12**, 1495 (1975).
[79] M. Lacombe, B. Loiseau, J. M. Richard, R. Vinh Mau, J. Côté, P. Pirès, and R. de Tourreil, Phys. Rev. C **21**, 861 (1980).
[80] M. Lacombe, B. Loiseau, R. Vinh Mau, J. Côté, P. Pirès, and R. de Tourreil, Phys. Lett. **101B**, 139 (1981).
[81] J. M. Laget, private communication.
[82] G. Beck and H. Arenhövel, Few Body Syst. **13**, 165 (1992).
[83] E. Hummel and J. A. Tjon, Phys. Rev. C **42**, 423 (1990); report, 1993.
[84] E. Hummel and J. A. Tjon, Phys. Rev. Lett. **63**, 1788 (1989).
[85] M. van der Schaar, Ph.D. thesis, Rijksuniversiteit, Utrecht, The Netherlands, 1991.